Modelling of water evaporation from cracked clayey soil

Wei-Kang Song, Yu-Jun Cui

Modelling of water evaporation from cracked clayey soil

Wei-Kang SONG[a], Yu-Jun CUI[b]

a: School of Civil Engineering, Zhengzhou University, Zhengzhou, China

b: Ecole des Ponts ParisTech, Laboratoire Navier/CERMES, 6-8, av. Blaise Pascal, 77455 Marne-la-Vallée, France

Corresponding Author:

Prof. Yu-Jun CUI
Ecole des Ponts ParisTech
6-8 av. Blaise Pascal, Cité Descartes, Champs-sur-Marne
77455 MARNE LA VALLEE
France
Telephone: +33 1 64 15 35 50
Fax: +33 1 64 15 35 62
E-mail: yu-jun.cui@enpc.fr

Abstract:

A model for predicting water evaporation from clayey soil with desiccation cracks was developed based on a general suction-related model. The effect of desiccation cracks was accounted for by introducing a surface crack ratio (R_c) and a ratio of relative humidity in cracks to that at soil surface (k). The model was validated on the basis of two large scale evaporation experiments in an environmental chamber under controlled atmospheric condition. The results show that soil cracking strongly affects the actual evaporation rate, especially after the falling-rate evaporation stage. Ratios R and k are two relevant parameters in describing the effect of cracks on water evaporation in a simple fashion. The introduction of these two parameters allows the three-dimension evaporation problem in cracked soil to be reduced to one-dimension evaporation problem. Comparison between the model predictions and the experimental results shows that with consideration of the effect of desiccation cracks, the model can satisfactorily describe water evaporation from cracked clayey soil under controlled atmospheric condition.

Key words: cracked clayey soil; actual evaporation rate; suction-based model; surface crack ratio

Notations

a	Fitting parameter
A	Soil evaporation surface area
e	Base of natural logarithm, equal to 2.71828
E_a	Actual evaporation rate
E_p	Potential evaporation rate
h	Relative humidity
h_a	Air relative humidity at a reference height
h_{a_in}	Absolute humidity at inlet of the chamber
h_{a_out}	Absolute humidity at outlet of the chamber
h_s	Relative humidity at soil evaporating surface
$h_{\_crack}$	Relative humidity induced by water vapor from cracks
$h_{\_non\text{-}crack}$	Relative humidity induced by water vapor from non-cracked soil
$h_{\_surface}$	Soil surface relative humidity
k	Ratio of relative humidity in cracks to that at soil surface
m	Fitting parameter
n	Fitting parameter
q	Air flow rate passing through the chamber
R	Universal constant, equal to 8.31432 J/mol/K
R_c	Surface crack ratio, equal to the surface area of cracks over the total initial surface area of the drying soil column
T	Temperature

u	Wind speed at 50-mm height over soil/water surface
W	Water molecular weight, equal to 18.016 g/mol
α	Constant determined through evaporation experiment
β	Constant determined through evaporation experiment
θ_r	Residual Volumetric water content
θ_s	Saturated volumetric water content
θ_w	Volumetric water content
ρ_w	Water density
φ	Soil suction

1. Introduction

Water evaporation from clayey soil causes decrease of soil water content and increase of soil suction, and hence induces desiccation cracks and changes in hydro-mechanical behaviour of soil, giving rise to possible damage of geotechnical structures such as pavements, embankments and shallow foundations of buildings (Corti et al., 2011; Puppala et al., 2011; Harrison et al., 2012; Jahangir et al., 2013; Fernandes et al., 2015; Wang et al., 2016), instability of slopes (Baker, 1981; Tang et al., 2011, 2016), and landslide (Sharma and Nakagawa, 2010). For addressing these problems, it is essential to well understand the soil water content and suction evolutions by considering the soil-atmosphere interaction.

In the attempt of well describing the soil water evaporation process, more and more attention has been paid to the prediction of changes in soil temperature, suction and water content, the main parameters defining the boundary condition at soil-atmosphere interface (An et al., 2017, 2018; Teng et al., 2014, 2016). Considering that the evaporation process is triggered by the vapor pressure deficit which occurs between evaporating surface and atmosphere, the mass transfer model (*i.e.* Dalton type equation) was proposed for predicting water evaporation from water or wet soil surface (Wilson et al., 1994, 1997). The evaporating surface temperature, the temperature and relative humidity at surrounding air are involved in this model. It can be used to calculate evaporative fluxes when combined with the liquid water and water vapor flow transient equations and the heat transfer equation (Wilson et al.,

1994). Note that the mass transfer coefficient shows a strong correlation with the wind velocity (Gerard et al., 2016). In addition to the vapor pressure deficit mentioned above, the mass and energy balance also exist at the soil-atmosphere interface. Thus, the water balance model and energy balance model (Blight, 1997; Cui and Zornberg, 2008; Cui et al., 2010) were both used to predict the water loss through evaporation, supposing that the related parameters such as infiltration rate, runoff rate, interception, net radiation flux, soil heat flux and sensible heat flux are known. Furthermore, after introducing a wind function into the mass transfer model and using the air temperature to calculate the saturated vapor pressure, Penman (1948) proposed a model which is the combination of mass transfer model and the energy balance model, allowing prediction of the water evaporation rate from vegetated and bare soil surfaces when the water supply is unlimited. However, it usually overestimates the evaporation rate when the soil becomes unsaturated (Wilson et al., 1997). In view of the physical meaning of water vapor traveling from soil to atmosphere, that is, water vapor is transported from evaporating surface to the soil surface by molecular diffusion and then be transferred from soil surface to the atmosphere through laminar or turbulent (Kondo et al., 1990), the resistance models were proposed by introducing the aerodynamic resistance and soil resistance (Mahfouf and Noilhan, 1991; Daamen and Simmonds, 1996; Yamanaka et al., 1997). Additionally, in order to take into account the appearance of dry soil layer during evaporation, Aluwihare and Watanabe (2003) proposed a model involving the dry layer height. However, the determination of soil resistance is still a challenge of this model. Later, Smits et al. (2011) proposed

a numerical model to simulate coupled heat, water vapor, and liquid water flux through sandy soil and the application of this model also shows the strong effect of the dry soil layer on the evaporation process (Smits et al., 2012). Assuming that the potential evaporation rate is known, Campbell (1985) proposed a simple formula only involving relative humidity of soil and air to determine the actual evaporation rate, based on both the atmosphere and soil parameters. According to Kelvin's equation, the soil surface relative humidity can be replaced by the suction at the same position, leading to the suction-related model (Wilson et al., 1997; Ta, 2009). Note that this model is independent of soil nature (e.g., soil texture and mineralogy). Song et al. (2018) extended the suction-related model by introducing a relative humidity distribution function. In addition to the models mentioned above, many researchers also proposed different analytical or semi-analytical models on the basis of the Richards equation (Novak, 1988; Nasseri et al., 2012; Yamanaka and Yonetani, 1999; Teng et al., 2013, 2019). However, these models cannot well describe the evaporation mechanism and may become inapplicable when the liquid water becomes discontinue with a dry layer formed on soil surface. In this regard, Teng et al. (2019) proposed a physics-based analytical model which can describe the movement of the vaporization plane during evaporation.

The above-mentioned studies constituted a solid basis for analyzing the process of water evaporation from soils. However, the important effect of cracks to water evaporation from clayey soil was rarely investigated, even though it is well

documented that cracks could greatly contribute to water evaporation due to the relatively high water content of soil in the vicinity of cracks (Adams and Hanks, 1964; Selim and Kirkham, 1970; Ritchie and Adams, 1974).

In this study, a new evaporation rate prediction model was developed for investigating water evaporation from cracked clayey soil surface based on the general suction-related model (see Campbell, 1985; Wilson et al., 1997; Ta, 2009 and Song et al., 2018). The effect of desiccation cracks was accounted for by introducing the surface crack ratio (R_c) (*i.e.* the ratio of the surface area of cracks to the total initial surface area of the drying soil column) and the ratio of relative humidity in cracks to that at soil surface (k). All the model parameters were determined using the data from two large scale evaporation experiments conducted by Song et al. (2016) and Song (2014). Comparison was made between calculation and measurement, showing the relevance of the model.

2. General suction-related model

As discussed by Song et al. (2018), the general suction-related model (Campbell, 1985; Wilson et al., 1997; Ta, 2009) considering both the atmosphere and soil effects on soil water evaporation process can be described as follows:

$$\frac{E_a}{E_p} = \frac{h_s - h_a}{100 - h_a} \quad (1)$$

$$\frac{E_a}{E_p} = \frac{h_{\_surface} - h_a}{100 - h_a} \quad (2)$$

where E_a and E_p are the actual and potential evaporation rates (mm/day), respectively;

126 h_s is the soil evaporating surface relative humidity (%); h_a is the air relative humidity
127 at a reference height (%) and $h_{\_surface}$ is the soil surface relative humidity (%).
128
129 Generally, h_s and $h_{\_surface}$ can be determined by Kelvin's equation (Eq. (3)):

130 $$h = \exp\left[-\frac{\varphi W\left(1/\rho_w\right)}{RT}\right] \quad (3)$$

131 where h is relative humidity (%); φ is soil suction (kPa), W is water molecular weight
132 (*i.e.* 18.016 g/mol), ρ_w is water density (*i.e.* 1000 kg/m^3 at 4 °C), R is the universal
133 constant (*i.e.* 8.31432 J/mol/K) and T is temperature (K).
134

135 ## 3. Modified suction-related model for cracked clayey soil

136 For a clayey soil, upon water evaporation, the soil suction increases, resulting in soil
137 shrinking and eventually soil cracking. Once the desiccation cracks formed, water can
138 evaporate into the atmosphere through two different ways: (1) directly from the
139 non-cracked soil surface; (2) from the desiccation cracks walls (Fig. 1). As shown in
140 Fig. 1, the relative humidity at the soil surface can be defined as $h_{\_surface}$. It constitutes
141 two parts: the relative humidity induced by water vapor from non-cracked soil
142 ($h_{\_non\text{-}crack}$) and the relative humidity induced by water vapor from cracks ($h_{\_crack}$).
143 Note that $h_{\_crack}$ is an equivalent relative humidity inside the desiccation cracks. When
144 the soil surface is becoming dry, the value of $h_{\_non\text{-}crack}$ is much lower than that of
145 $h_{\_crack}$. For simplicity, we assume:

146 $$h_{\_crack} = k h_{\_non\text{-}crack} \quad (4)$$

147 where k is the ratio of $h_{\_crack}$ to $h_{\_non\text{-}crack}$.

By considering the soil surface crack ratio (R_c), the ratio of the cracks area to the total initial surface area of the drying soil column (Tang et al., 2008), Eq. (5) can be obtained:

$$h_{\_surface} = R_c h_{\_crack} + (1 - R_c) h_{\_non\text{-}crack} \quad (5)$$

or $$h_{\_surface} = [1 + (k - 1)R_c] h_{\_non-crack} \quad (6)$$

From Eq. (2) and Eq. (6), the following expression can be deduced, allowing the calculation of water evaporation with consideration of effect of cracks:

$$\frac{E_a}{E_p} = \frac{[1+(k-1)R_c] h_{\_non-crack} - h_a}{100 - h_a} \quad (7)$$

Particularly, when the soil is extremely dry and the water evaporation rate is low, the water evaporates from the desiccation cracks makes greater contribution to the soil surface relative humidity than from the non-cracked soil. Thereby, in that case, assuming $h_{\_non\text{-}crack}$ is equal to h_a, we obtain:

$$h_{\_surface} = (1 + kR_c - R_c) h_a \quad (8)$$

It is noted that the unit in the equations mentioned above is percentage (%) for the relative humidity, and is in decimal for the surface crack ratio (R_c).

For the potential evaporation rate (E_p), it can be predicted using the model proposed and calibrated by Ta (2009) and Song et al. (2018) (Eq. (9)). Note that this model is derived from the general form of the existing mass transfer model (e.g., Singh and Xu, 1997) based on the results from six free water evaporation experiments under controlled atmospheric conditions (various wind speeds and air temperatures) (Song et al., 2018).

$$E_p = (\alpha + \beta u)(100 - h_a) \quad (9)$$

where E_p is the potential evaporation rate (mm/day); u is the wind speed at 50-mm height over soil/water surface (m/s); h_a is the corresponding air relative humidity at the same reference level as the wind speed (%); α and β are two constants determined through free water evaporation experiment with different wind speeds, *i.e.* the relationship between $E_p/(100-h_a)$ and the wind speed u (see Song, 2014). As shown in Fig. 2, the experimental data exhibit a quite large scatter. The linear best fitting of all data (Line 1) gives the values of α and β equal to 0.022 and 0.031, respectively. If the largest data and the smallest data are considered, the linear best fittings (Line 2 and Line 3) gives the range of α from 0.014 to 0.032, and the range of β from 0.025 to 0.037.

4. Evaporation experiments on clayey soil

4.1 Materials

The clayey soil used for investigating soil water evaporation process was taken from an experimental embankment in Héricourt, France. Its geotechnical properties were investigated by Song et al. (2016), and are presented in Table 1.

4.2 Experimental set-up

The soil water evaporation test was conducted in an environmental chamber system proposed by Song et al. (2014). This environmental chamber system (see Fig. 3) contains a model test chamber filled with soil sample and equipped with various sensors for measuring both soil and atmosphere parameters, a wind simulating unit, an

192 air collection unit, an image capture unit, a water supply unit, and a data logging unit.
193 During the evaporation test, cool air was firstly heated and controlled by the wind
194 simulating unit, forming hot wind with different temperatures and speeds. Then, the
195 hot air passed through the model test chamber and removed the water vapor from soil
196 surface. Finally, the moist air was gathered in the air collection unit. It is noted that
197 the air temperature and relative humidity were measured before and after passing
198 through the chamber, being used for determining the actual evaporation rate.
199 Furthermore, the soil surface desiccation crack was monitored by the image capture
200 unit every 90 min; the water table at soil bottom was also kept constant using the
201 water supply unit during the whole evaporation test. All data were recorded by the
202 data logging unit.
203
204 *4.3 Test procedure*
205 The soil sample transported from the embankment construction site was firstly air
206 dried in the laboratory, and then crushed and passed through 2 mm sieve. Finally, it
207 was stored in sealed containers for further testing (Fig. 4(a)). Then, a gravel layer with
208 6.5 mm in thickness was compacted at the bottom of the chamber and covered by two
209 geotextile layer at both the surface and bottom of it, being termed as the drainage
210 layer. After that, the dry soil sample with the gravimetric water content of 6.4% was
211 compacted manually in layers to a target height of 250 mm corresponding to a dry
212 density of 1.4 Mg/cm^3 (Fig. 4(b)). In the meantime, various sensors measuring both
213 the atmospheric conditions (e.g., the air temperature, the air relative humidity, the

wind speed and the air flow rate) and the soil response (e.g., the soil matric suction, the soil temperature and the soil volumetric water content) were installed at various positions of the environmental chamber or buried in the soil at different depths (Figs. 4(c) and 4(d)). Furthermore, a camera was hung over the soil surface at a certain elevation, enabling the soil surface desiccation cracks to be monitored over time (Fig. 4(e)). Finally, the soil sample was saturated by the water supply unit and then the evaporation experiment was started under controlled atmospheric condition (Fig. 4(f)).

As for the evaporation experiment, two controlled atmospheric conditions in terms of air relative humidity, temperature and air flow rate were applied to the soil sample (Table 2); the water table at its bottom (250 mm below the soil surface) was also kept constant. The durations of the two experiments were 83 days and 41 days, respectively.

For the actual evaporation rate, it was determined using the formula proposed by Mohamed et al. (2000) and Aluwihare and Watanabe (2003), based on the measurement of atmospheric parameters at the inlet and outlet of the chamber, as follows:

$$E_{\mathrm{a}} = 86400\,\frac{q(h_{a\_out}-h_{a\_in})}{\rho_{\mathrm{w}}A} \tag{10}$$

where E_a is the actual evaporation rate (mm/day), $h_{\mathrm{a\_out}}$ and $h_{\mathrm{a\_in}}$ are the absolute humidity at outlet and inlet of the chamber, respectively (Mg/m^3), q is the air flow rate

236 passing through the chamber (L/s), ρ_w is the water density (Mg/m^3) and A is the soil
237 evaporation surface area (m^2).
238
239 The surface crack ratio (R_c) was used to describe the evolution of desiccation cracks.
240 It was determined using the photographs of soil surface taken with the fixed time
241 interval (*i.e.* 90 min) by applying the digital image processing technique proposed by
242 Tang et al. (2008). Specifically, the original color image of surface crack pattern from
243 the image capture unit was firstly changed to the grey one, and then it was converted
244 into a binary black and white image through the binarisation process. Note that the
245 black zone in this binary image represented the crack and the white zone indicated the
246 soil aggregate without crack. Finally, the ratio of the area of black zone to the total
247 zone was determined using the software CIAS (Tang et al., 2008), that is, the value of
248 R_c. More details about this digital image processing technique can be found in Tang et
249 al. (2008).
250
251 *4.4 Typical results*
252 The relationship between the volumetric water content and soil suction at different
253 depths (*i.e.* 15, 20, 25, 77 and 173 mm depths) during the two experiments is
254 presented in Fig. 5 (Song, 2014; Song et al., 2016). At the same time, due to the
255 incomplete data, a fitting curve which covers the suction range being obtained in these
256 tests (*i.e.* less than 1.5 MPa) is described by the model proposed by Fredlund and
257 Xing (1994) (see Eq. (10)).

$$\theta_w = \theta_r + \frac{\theta_s - \theta_r}{\{\ln[e+(\varphi/a)^n]\}^m} \quad (11)$$

where θ_w is the volumetric water content (%); θ_s is the saturated volumetric water content (%); θ_r is the volumetric water content at residual state (%); φ is the soil suction (kPa); e is 2.71828, *i.e.* the base of natural logarithm; a, m and n are three fitting parameters, respectively.

The actual and potential evaporation rates calculated using Eqs. (10) and (9) are shown in Fig. 6. It can be observed that the actual evaporation values initially kept at a relative stable level (*i.e.* the constant-rate stage) around 2.3 mm/day (Test 1 and Test 2), then decreased sharply (*i.e.* the falling-rate stage) and reached a new stable level (*i.e.* slow-rate stage) around 0.3 mm/day for Test 1 and 0.8 mm/day for Test 2. For the potential evaporation rate, it increased over time due to the decrease of air relative humidity. Notably, Test 2 started with six free water evaporations; therefore, the soil water evaporation started after t = 12.8 days.

Figure 7 shows the evolutions of surface crack ratio (R_c) and actual evaporation rate during two evaporation tests. It appears from this figure that the R_c increased with the decrease of actual evaporation rate and reached a stable value of 25.5 % in Test 1 and 29.0 % in Test 2. The decrease of evaporation rate lagged behind that of the evolution of R_c, reflecting the effect of cracks on water evaporation, that is, providing water vapor and thus delaying the decrease of evaporation rate. Note that the calculation of surface crack ratio in this study considered the gap between the wall of chamber and

the soil body, because water vapor could migrate to the atmosphere through this gap, affecting the total evaporation rate.

More details about the two experiments can be found in Song et al. (2016).

5. Determination of parameters

The ratio E_a/E_p can be determined using the measured actual evaporation rate and the calculated potential evaporation rate for the two evaporation tests (see Fig. 6). Generally, due to the sufficient water supply to the evaporation process, the value of E_a/E_p is equal to 1 during the constant-rate evaporation stage. However, as shown in Fig. 6, the potential evaporation rate was lower than the actual one during this stage and thus E_a/E_p was not equal to 1. This was due to the accuracy of the determination of parameters α and β in Eq. (9), indicating the necessity of adjusting the potential evaporation rate calculated using Eq. (9) (Song et al., 2018). In a simple way, E_p was multiplied by a constant (1.15 for Test 1 and 1.2 for Test 2), leading the average value of E_a/E_p during the constant-rate evaporation stage to 1. The corresponding values of α and β were 0.028 and 0.027 in Test 1, and were 0.029 and 0.031 in Test 2, falling in the ranges of α and β determined previously from Fig. 2. This justified the modification made on E_p.

To determine parameter k, the surface relative humidity ($h_{\_surface}$) was firstly predicted using Eq. (2) with the adjusted potential evaporation rate, measured actual

302 evaporation rate and the relative humidity at 50-mm height and then compared with
303 the relative humidity measured at 50-mm height (see Fig. 8). Then, parameter k could
304 be calculated by Eq. (8) with the known surface crack ratio (Fig. 7). For Test 1, the
305 data shown in Fig. 8(a) from t = 65 days to t = 84 days were selected for the
306 determination of k. Note that the R_c value during this stage was 25.5 %. A value of
307 3.65 was obtained for k. For Test 2, the data shown in Fig. 8(b) from t = 43 days to t =
308 54 days were selected for the determination. The corresponding R_c value was 29 %
309 and a value of k = 5.59 was obtained. Note that the value of k was larger in Test 2 than
310 in Test 1, owing to more water vapor that entered the atmosphere through the deeper
311 zone in Test 2. Indeed, the direct measurement of the width and depth of desiccation
312 crack at the end of the two tests showed that the depths of cracks in Test 2 were
313 deeper than in Test 1 (see Fig. 9).
314
315 As observed in Fig. 8, the soil surface relative humidity deduced from Eq. (2) was
316 much higher than at 50-mm height, even at the end of the evaporation process. As
317 shown in Fig. 6, the actual evaporation rate at the slow-rate evaporation stage was
318 extremely low. Basically, once the evaporation rate was close to stabilization, the
319 relative humidity at the soil surface approached the one in the air. The phenomenon
320 observed in Fig. 8 might be attributed to the occurrence of desiccation cracks during
321 the soil water evaporation process, *i.e.* the cracks allowed water to evaporate from the
322 walls of them, increasing the relative humidity at the soil surface and converting the
323 one-dimension evaporation model (*i.e.* water evaporates only from the soil surface)

into the three-dimension one (*i.e.* water evaporates from both the soil surface and the crack walls). This indicated the strong effect of cracks on the evaporation process. Furthermore, we could deduce that predicting actual evaporation rate directly using Eqs. (1) or (2) was not appropriate for cracked soils.

6. Verification of the proposed model

After determining the related parameter of the proposed model (*i.e.* Eq. (7)), two methods (Method 1 and Method 2) were used for the verification. The details of the two methods are described as follows and the results from Test 1 were taken as an example firstly. The diagram of the two methods is shown in Fig. 10.

In Method 1, the volumetric water content at the soil surface (Fig. 11) was firstly extrapolated from the water content profile obtained from the evaporation test (see Song et al., 2016). Then, the soil surface suction was determined using the water retention curve fitted by the model proposed by Fredlund and Xing (1994) (Eq.(11)) (see Fig. 5(a)). In this model, the saturated volumetric water content (θ_s) was determined by averaging the initiation water content at different depths and was equal to 58.8% and the residual volumetric water content (θ_r) was estimated to be 11.6 %, *i.e.* the water content at 25-mm depth at the end of test. For the 3 fitting parameters *a*, *n* and *m*, they were 50, 0.55 and 25, respectively. After that, the suction at soil surface was transformed into the surface relative humidity by Kelvin's equation (Eq. (3)). Notably, this surface relative humidity corresponded to the one at the soil surface

346 without cracks, *i.e.* $h_{\_non\text{-}crack}$ in Eq. (7). Finally, with the determined R_c, k, $h_{\_non\text{-}crack}$,
347 E_p and h_a, the actual evaporation rate (E_a) could be calculated using Eq. (7) (Fig. 12).
348 Notably, as the water retention curve only involved suctions lower than 1.5 MPa (*i.e.*
349 the range of the high-capacity tensiometor for measuring soil matric suction, see Song
350 et al., 2013, 2014), the prediction of actual evaporation rate was conducted in the first
351 15 days. As can be seen in Fig. 12, large difference existed between the measured
352 value and the one predicted by Method 1, which could be attributed to the possible
353 inaccurate determination of the water retention curve for the surface soil. Indeed,
354 large heave was observed at the surface of the soil sample during the saturation
355 process, leading to a dry density of soil in surface zone lower than the one at deeper
356 zone. Thus, predicting the actual evaporation rate using water retention curve deduced
357 from the experimental data in deeper zone rather than from the surface was
358 unreasonable. Furthermore, the water retention curve which covered the full suction
359 range was also needed for a better evaporation prediction. In addition to the factors
360 mentioned above, the effect of desiccation cracks was also required to be taken into
361 account. Indeed, for a large scale cracked soil sample, the water content distribution at
362 soil surface is quite complicated and hence the water retention curve is also difficult
363 to determine.
364
365 In order to address the problems with Method 1, Method 2 was introduced with an
366 equivalent water retention curve at soil surface and a modified surface volumetric
367 water content. In this method, the cracked surface soil was assimilated to a thin layer

without cracks by introducing parameters R_c and k, allowing the three-dimension evaporation problem in cracked soil to be reduced to one-dimension evaporation problem. Firstly, the relative humidity at the non-cracked soil surface (*i.e.* the equivalent thin soil layer) was determined by Eq. (7) with the measured data and the values of k and R_c. Note that this was an equivalent surface relative humidity and was equal to $h_{\_non\text{-}crack}$. Then, the corresponding surface suction (*i.e.* equivalent surface suction) was calculated using Kelvin's Equation (Fig. 13). Afterwards, the equivalent water retention curve (Fig. 14) was determined by the equivalent surface suction and the surface volumetric water content extrapolated from the water content profile during the evaporation process (see Fig. 11). This curve was also fitted by the model proposed by Fredlund and Xing (1994) (Eq. (11)). The saturated volumetric water content (θ_s) and the residual volumetric water content (θ_r) were determined by the extrapolated surface volumetric water content, *i.e.* 66 % for the saturated one and 2.2 % for the residual one. For the corresponding fitting parameters a, n and m, they were 50, 1.9 and 9, respectively. As shown in Fig. 14, large fluctuation was observed in the high suction range, which could be attributed to the inaccurate determination of water content when cracks developed. As a matter of fact, the development of desiccation cracks led the volumetric water content sensor to expose to the air partly or totally, leading to unreliable results (see Fig. 15). Furthermore, the suction used in this water retention curve took the effect of cracks into account. Therefore, it is better to consider this effect when determining the surface volumetric water content. Thereby, the equivalent surface volumetric water content (Fig. 11) was calculated using the

equivalent surface suction (Fig. 13) and the water retention curve (Fig. 14). As shown in Fig. 11, the equivalent surface volumetric water content thus determined was in accordance with the one extrapolated from the water content profile before most cracks were formed (e.g., t = 15 days), indicating the rationality of the method proposed which considered the crack development. Therefore, the modified surface water content could be divided into two stages: (1) Stage 1: the value was equal to the one extrapolated from the water content profile (in the first 15 days); and (2) Stage 2: the corresponding value was replaced by the equivalent one after most desiccation cracks being formed. Note that the time t = 15 days corresponded to the end of the constant-rate evaporation stage. Afterwards, the modified surface volumetric water content was used to determine the surface suction with the equivalent water retention curve. Hence, the relative humidity at soil surface (*i.e.* $h_{\text{\_non-crack}}$) could be obtained by Kelvin's equation. Finally, with the determined parameters k, R_c, h_a, $h_{\text{\_non-crack}}$ and E_p, the actual evaporation rate (E_a) was determined by Eq. (7). It appeared from Fig. 12 that the predicted actual evaporation rate by Method 2 agreed well with the measured one during evaporation experiment.

The relevance of the proposed model was also verified using the experiment data obtained from Test 2. For clarity, only Method 2 was adopted for this purpose. Firstly, an equivalent water retention curve was determined based on the experiment data obtained during Test 2 (Fig. 16). The equivalent water retention curve was also fitted by the model proposed by Fredlund and Xing (1994) (see Eq. (11)). More specifically,

412 the volumetric water content at saturated state (θ_s) was 67 %, and the volumetric
413 water content at residual state (θ_r) was 2.2 %. Furthermore, as for the related fitting
414 parameters a, n and m, they were 45, 1.5 and 7, respectively. Notably, no large
415 difference was identified in high suction range, as shown in Fig. 16. This is because of
416 the more significant development desiccation cracks in Test 2, allowing water content
417 in the surface zone to be more homogeneous over depth. Then, the surface volumetric
418 water content was modified by the equivalent one (Fig. 17). The modified surface
419 volumetric water content included two parts: the one directly extrapolated from the
420 water content profile (before t = 19 days, *i.e.* constant-rate evaporation rate stage) and
421 the second part from the equivalent one with the effect of most desiccation cracks
422 (after t = 19 days). Note that only the result of the extrapolated volumetric water
423 content before t = 27 days were shown in this figure, because the development of
424 cracks led to negative value when the water content profile was used. Afterwards, the
425 surface suction was determined by the equivalent water retention curve with the
426 modified surface water content and hence the corresponding surface relative humidity
427 could also be obtained using Kelvin's equation (see Figs. 18 and 19). Finally, with the
428 known k, R_c, h_a, $h_{\_non\text{-}crack}$ and E_p, the actual evaporation rate (E_a) could be determined
429 by Eq. (7). As can be seen in Fig. 20, the predicted evaporation rate was consistent
430 with the one measured during evaporation experiment, confirming the relevance of
431 the proposed model as well as the relevance of Method 2.
432

433 ## 7. Conclusions

434 A new water evaporation rate model considering the effect of desiccation cracks was

435 proposed for clayey soils based on the general suction-related model. The surface
436 crack ratio (R_c) and the ratio of relative humidity from cracks and that from
437 non-cracked soil (k) were introduced for this purpose. This new model (Eq. (7)) was
438 verified based on the test results of Song et al. (2016) and Song (2014).
439
440 The soil desiccation cracks provide new paths (*i.e.* the crack wall) for the water vapor
441 entering the atmosphere. This converts the one-dimension evaporation pattern (*i.e.*
442 water evaporates only from the soil surface) into a three-dimension one (*i.e.* water
443 evaporates from both the soil surface and the crack walls), strongly influencing the
444 evolution of actual evaporation rate, especially after the falling-rate evaporation stage.
445 R_c and k are two key parameters for describing the effect of desiccation cracks on the
446 water evaporation process. The introduction of the two parameters in the model
447 allows the water evaporation to be described only using the parameters for the soil
448 surface without specifically considering water evaporation from each crack. In other
449 words, the proposed model allows the three-dimension evaporation problem in
450 cracked soil to be reduced to a one-dimension problem. This is important while
451 applying the model to field condition because only parameters which can be easily
452 determined are needed.
453
454 Adopting an equivalent water retention curve for the surface soil with desiccation
455 cracks appeared to be successful. This allowed the effect of desiccation cracks in large
456 scale soil sample to be considered indirectly and the suction range to be extended.

Acknowledgments

The work is supported by the China Postdoctoral Science Foundation funded project (Grant No. 2018T110742, 2016M592312), the National Key R&D Program of China (Grant No. 2017YFC1502600), and the Key Scientific Research Project of the Higher Education Institutions of Henan Province (Grant No. 18A560024). The support by Ecole des Ponts ParisTech is also greatly acknowledged.

References

Adams, J.E., Hanks, R.J., 1964. Evaporation from soil shrinkage cracks. Soil Sci. Soc. Am. J. 28(1), 281-284.

An, N., Hemmati, S., Cui, Y.J., 2017. Numerical analysis of soil volumetric water content and temperature variations in an embankment due to soil-atmosphere interaction. Comput. Geotech. 83, 40-51.

An, N., Hemmati, S., Cui, Y.J., Tang, C.S., 2018. Numerical investigation of water evaporation from Fontainebleau sand in an environmental chamber. Eng. Geol. 234, 55-64.

Aluwihare, S., Watanabe, K., 2003. Measurement of evaporation on bare soil and estimating surface resistance. J. Environ. Eng. 129(12), 1157-1168.

Baker, R., 1981. Tensile strength, tension cracks, and stability of slopes. Soils Found. 21(2), 1-17.

Blight, D.E., 1997. Interactions between the atmosphere and the Earth. Géotechnique.

47(4), 715-767.

Campbell, G.S., 1985. Soil Physics with Basic: Transport Models for Soil-Plant systems. Elsevier, Amsterdam, Oxford.

Corti, T., Wüest, M., Bresch, D., Seneviratne S.I., 2011. Drought-induced building damages from simulations at regional scale. Nat. Hazards Earth Syst. Sci. 11(12), 3335-3342.

Cui, Y.J., Zornberg, J.G., 2008. Water balance and evapotranspiration monitoring in geotechnical and geoenvironmental engineering. Geotech. Geologic. Eng. 26(6), 783-798.

Cui, Y.J., Gao, Y.B., Ferber, V., 2010. Simulating the water content and temperature changes in an experimental embankment using meteorological data. Eng. Geol. 114, 456-471.

Daamen, C.C., Simmonds, L.P., 1996. Measurement of evaporation from bare soil and its estimation using surface resistance. Water Resour. Res. 32(5), 1393-1402.

Fredlund, D.G., Xing, A., 1994. Equations for the soil-water characteristic curve. Can. Geotech. J. 31(4), 521-532.

Fernandes, M., Denis, A., Fabre, R., Lataste, J.F., Chrétien, M., 2015. In situ study of the shrinkage-swelling of a clay soil over several cycles of drought-rewetting. Eng. Geol. 192, 63-75.

Gerard, P., Mpawenayo, R., Douzane, M., Debaste, F., 2016. Influence of climatic conditions on evaporation in soil samples. Environ. Geotech. https://doi.org/10.1680/jenge.15.00069.

501 Harrison, A.M., Plim, J.F.M., Harrison,M., Jones, L.D., Culshaw, M.G., 2012. The
502 relationship between shrink-swell ovvurrence and limate in south-East England.
503 Proc. Geol. Assoc. 123, 556-575.
504 Jahangir, E., Deck, O., Masrouri, F., 2013. An analytical model of soil-structure
505 interaction with swelling soils during droughts. Comput. Geotech. 54, 16-32.
506 Kondo, J., Saigusa, N., Sato, T., 1990. A parameterization of evaporation from bare
507 soil surfaces. J. Appl. Meteor. 29(5), 385-389.
508 Mahfouf, J.F., Noilhan, J., 1991. Comparative study of various formulations of
509 evaporation from bare soil using in situ data. J. Appl. Meteor. 30(9), 1354-1365.
510 Mohamed, A.A., Sasaki, T., Watanabe, K., 2000. Solute transport through unsaturated
511 soil due to evaporation. J. Environ. Eng. 126(9), 842-848.
512 Nasseri, M., Daneshbod, Y., Pirouz, M.D., Rakhshandehroo, G.R., Shirzad, A., 2012.
513 New analytical solution to water content simulation in porous media. J. Irrig. Drain.
514 Eng. 138(4), 328-335.
515 Novak M.D., 1988. Quasi-analytical solutions of the soil water flow equation for
516 problems of evaporation. Soil Sci. Soc. Am. J. 52(4), 916-924.
517 Penman, H. L., 1948. Natural evaporation from open water, bare soil and grass. Proc.
518 Roy. Soc. A. 193(1032), 120-145.
519 Puppala, A.J., Manosuthkij, T., Nazarian, S., Hoyos, L.R., 2011. Threshold moisture
520 content and matric suction potentials in expansive clays prior to initiation of
521 cracking in pavements. Can. Geotech. J. 48(4), 519-531.
522 Ritchie, J.T, Adams, J.E. Field measurement of evaporation from soil shrinkage

523 cracks. Soil Sci. Soc. Am. J. 38(1), 131-134.
524 Selim, H.M, Kirkham, D., 1970. Soil temperature and water content changes during
525 drying as influenced by cracks: A laboratory experiment. Soil Sci. Soc. Am. J. 34(4),
526 565-569.
527 Sharma, R. H., Nakagawa, H., 2010. Numerical model and flume experiments of
528 single- and two-layered hill slope flow related to slope failure. Landslides. 7(4),
529 425-432.
530 Singh, V.P, Xu, C.Y. Evaluation and generalization of 13 mass-transfer equations for
531 determining free water evaporation. Hydrol. Process. 11(3), 311-323.
532 Smits, K. M., Cihan, A., Sakaki, T., Illangasekare, T. H., 2011. Evaporation from soils
533 under thermal boundary conditions: Experimental and modeling investigation to
534 compare equilibrium- and nonequilibrium based approaches. Water Resour. Res. 47,
535 W05540.
536 Smits, K. M., Ngo, V.V., Cihan, A., Sakaki, T., Illangasekare, T. H., 2012. An
537 evaluation of models of bare soil evaporation formulated with different land surface
538 boundary conditions and assumptions. Water Resour. Res. 48, W12526.
539 Song, W.K., Cui, Y.J., Tang, A.M., Ding, W.Q., 2013. Development of a large scale
540 environmental chamber for investigating soil water evaporation. Geotech. Test. J.
541 36(6), 847-857.
542 Song, W. K., Cui, Y. J., Tang, A.M., Ding, W. Q., Tran, T.D., 2014. Experimental
543 study on water evaporation from sand using environmental chamber. Can. Geotech.
544 J. 51(2), 115-128.

545 Song, W. K., Cui, Y. J., Tang, A.M., Ding, W. Q., Wang, Q., 2016. Experimental study
546 on water evaporation from compacted clay using environmental chamber. Can.
547 Geotech. J. 53 (8), 1293-1304.
548 Song, W. K., Cui, Y. J., Ye, W.M., 2018. Modelling of water evaporation from bare
549 sand. Eng. Geol. 233, 281-289.
550 Song, W. K., 2014. Experimental investigation of water evaporation from sand and
551 clay using an environmental chamber. PhD. Thesis. Unversité Paris-Est, Paris.
552 Ta, A.N., 2009. Etude de l'interaction sol-atmosphere en chambre environmentale.
553 PhD. Thesis. Ecole des Ponts Paristech, Paris.
554 Tang, C.S., Shi, B., Liu, C., Zhao, L., Wang, B., 2008. Influencing factors of
555 geometrical structure of surface shrinkage cracks in clayey soils. Eng. Geol. 101,
556 204-217.
557 Tang, C.S., Shi, B., Liu, C., Gao, L., Inyang, H.I., 2011. Experimental investigation of
558 the desiccation cracking behavior of soil layers during drying. J. Mater. Civil Eng.
559 23(6), 873-878.
560 Tang, C.S., Wang, D.Y., Shi, B., Li, J., 2016. Effect of wetting-drying cycles on
561 profile mechanical behavior of soils with different initial conditions. Catena. 139,
562 105-116.
563 Teng, J., Yasufuku. N., Liu, Q., Liu, S., 2013, Analytical solution for soil water
564 redistribution during evaporation process. Water Sci. Technol. 68(12), 2545-2551.
565 Teng, J., Yasufuku, N., Liu, Q., Liu, S., 2014. Experimental evaluation and
566 parameterization of evaporation from soil surface. Nat. Hazards. 73(3), 1405-1418.

567 Teng, J., Yasufuku, N., Zhang, S., He, Y., 2016. Modelling water content
568 redistribution during evaporation from sandy soil in the presence of water table.
569 Comput. Geotech. 75, 210-224.
570 Teng, J., Zhang, X., Zhang, S., Zhao, C., Sheng, D., 2019. An analytical model for
571 evaporation from unsaturated soil. Comput. Geotech. 108, 107-116.
572 Wang, D.Y., Tang, C.S., Cui, Y.J., Shi, B., Li, J., 2016. Effects of wetting-drying
573 cycles on soil strength profile of a silty clay in micro-penetrometer tests. Eng. Geol.
574 206, 60-70.
575 Wilson, G.W., Fredlund, D.G., Barbour, S.L. 1994. Coupled soil-atmosphere
576 modeling for soil evaporation. Can. Geotech. J. 31(2), 151-161.
577 Wilson, G.W., Fredlund, D.G., Barbour, S.L., 1997. The effect of soil suction on
578 evaporative fluxes from soil surfaces. Can. Geotech. J. 34(1), 145-155.
579 Yamanaka, T., Takeda, A., Sugita, F., 1997. A modified surface-resistance approach
580 for representing bare-soil evaporation: Wind tunnel experiments under various
581 atmospheric conditions. Water Resour. Res. 33(9), 2117-2128.
582 Yamanaka, T., Yonetani, T., 1999. Dynamics of the evaporation zone in dry sandy
583 soils. J. Hydrol. 217, 135-148.

584 **List of Tables**

587

588 **List of Figures**

618 **Table 1.** Physical properties of the soil studied (Song et al., 2016).

619

Physical properties	Values
Specific gravity	2.7
Plastic limit (%)	37
Liquid limit (%)	76
Plastic index	39
Clay (＜2μm) content (%)	78

620 **Table 2.** Evaporation test conditions.

621

Test number	Air flow rate (L/min)	Temperature in heating tube (°C)	Average wind speed m/s	Test duration (days)
1	155±5	200	0.4	83
2	140±5	200	0.36	41

622

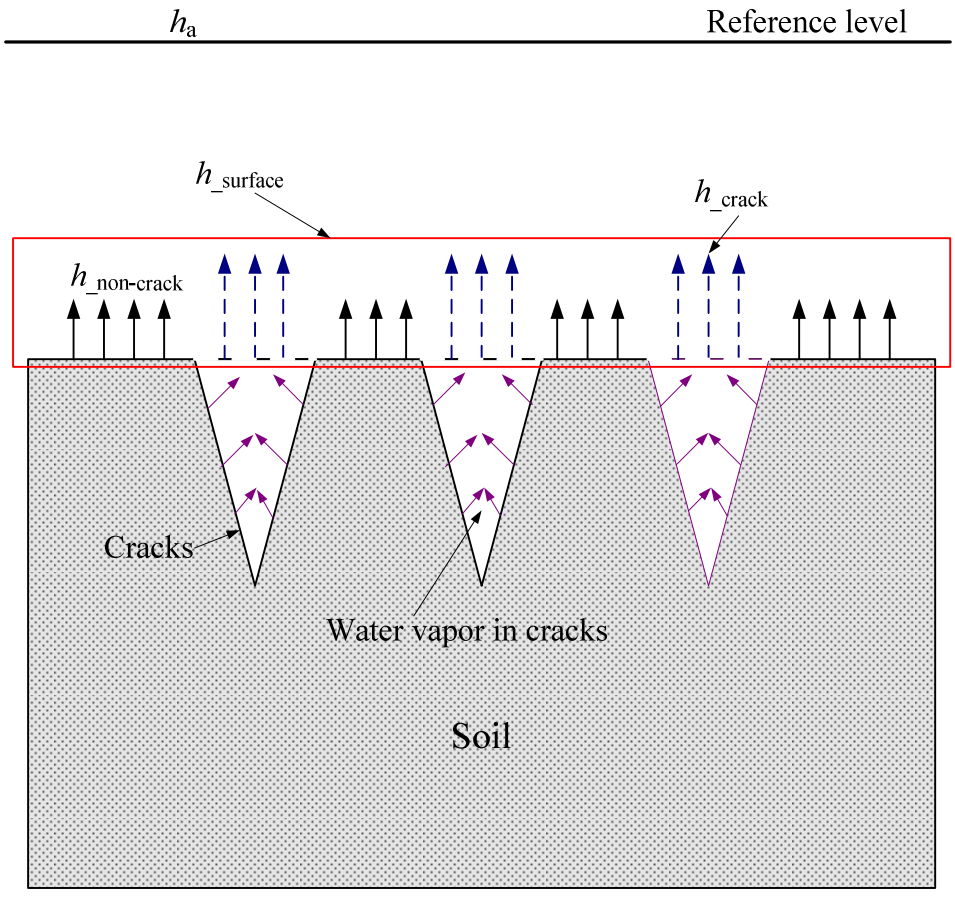

623

624 **Fig. 1.** Sketch of water evaporation from cracked soil.

625

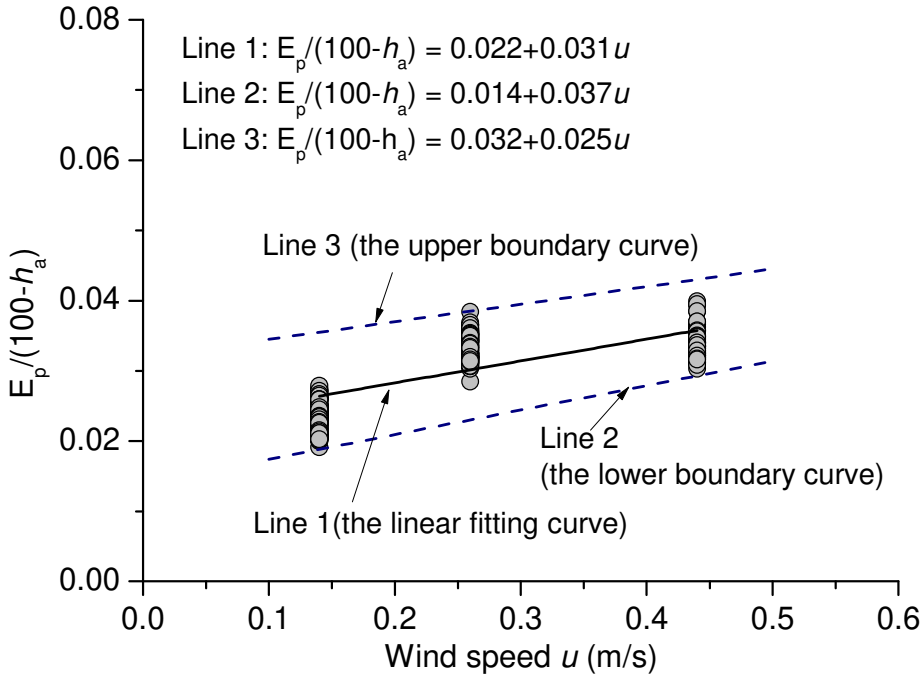

626

627 **Fig. 2.** The determination of parameters α and β.

628

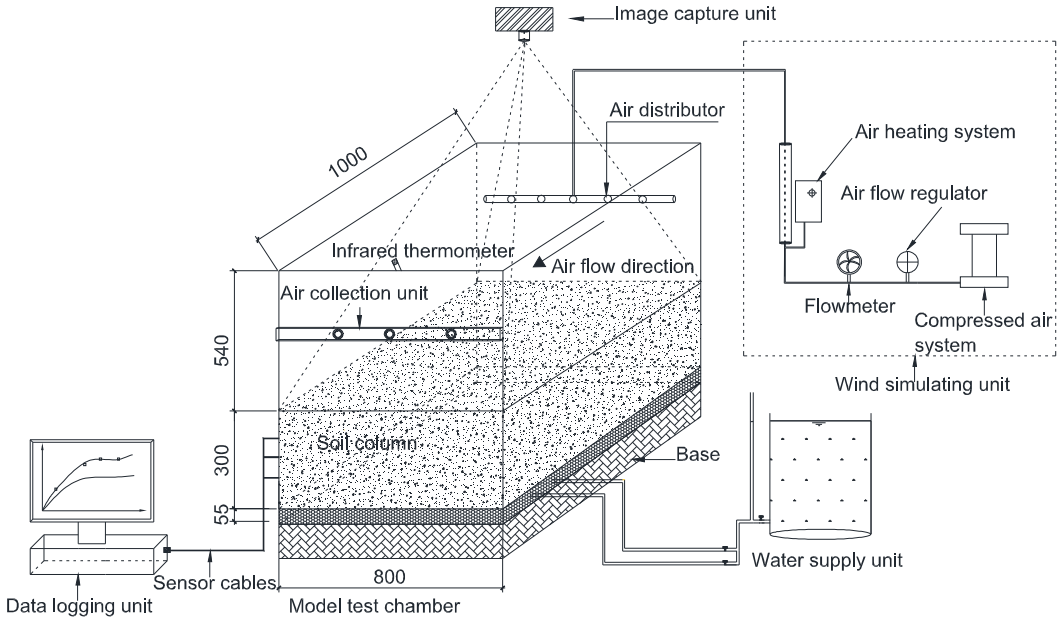

Fig. 3. Sketch of water evaporation environmental chamber system (after Song et al., 2016).

634

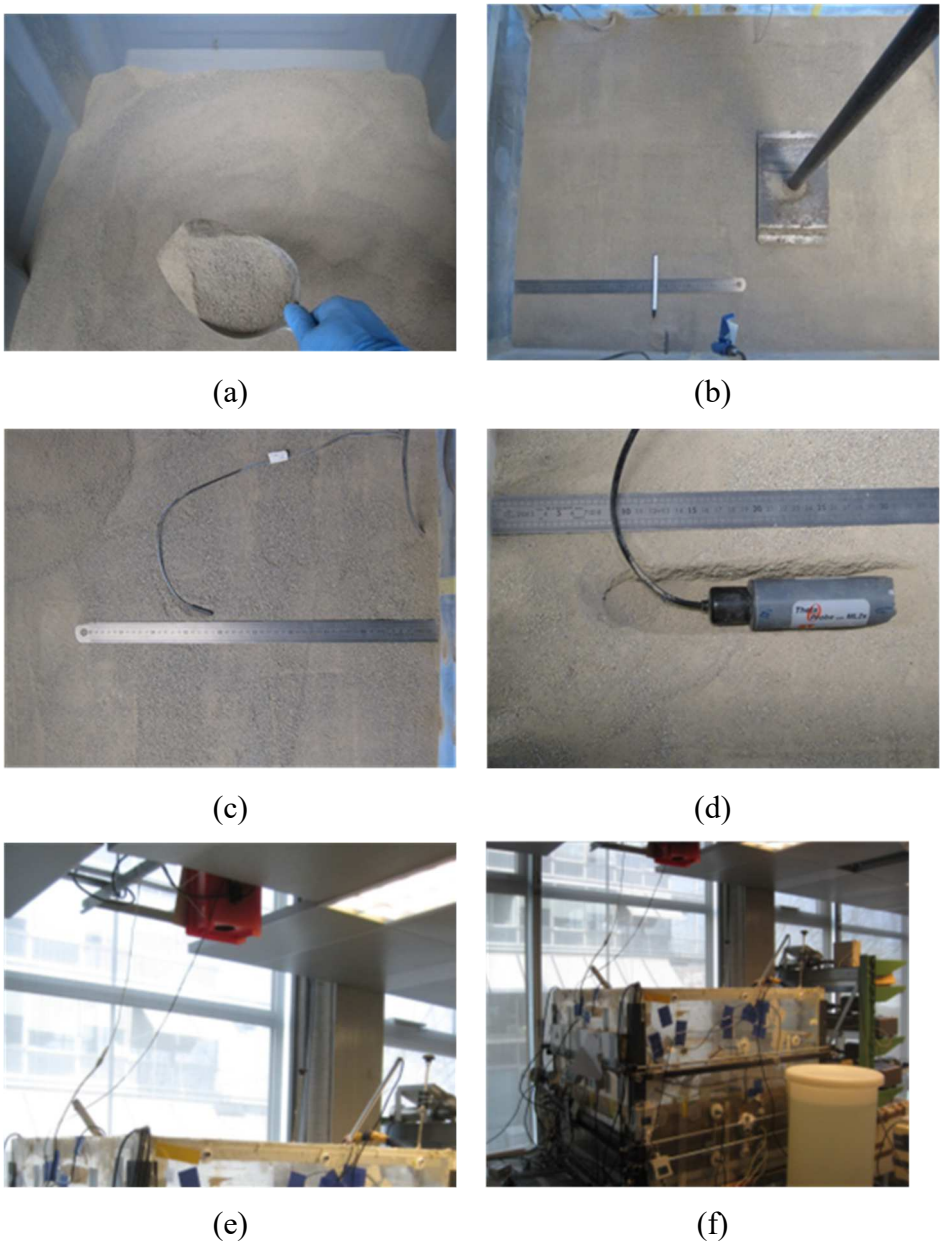

635 **Fig. 4.** Experimental procedure: (a) air-dried soil sample preparation, (b) soil
636 compaction, (c) soil temperature sensor installation, (d) volumetric water content
637 sensor installation, (e) camera installation, and (f) evaporation test initiation.

638

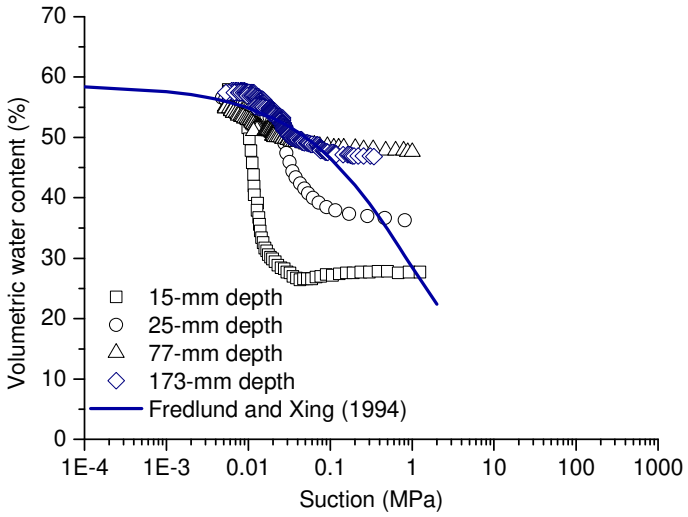

(a)

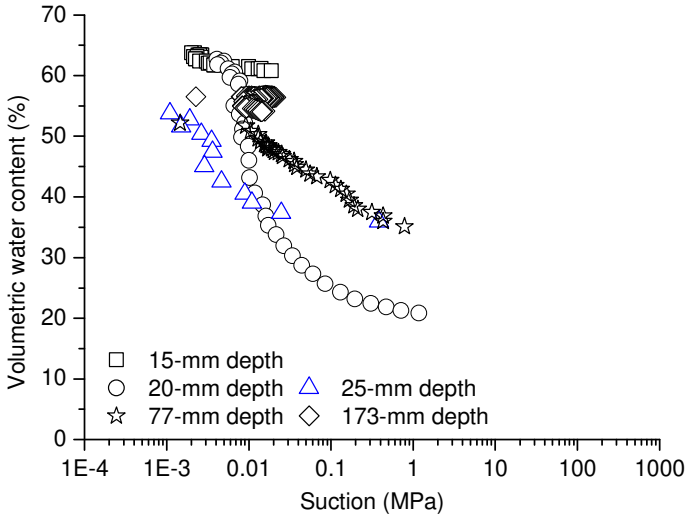

(b)

639 **Fig. 5.** Soil water retention curves obtained from evaporation tests: (a) Test 1, (b) Test

640 2.

641

642

643

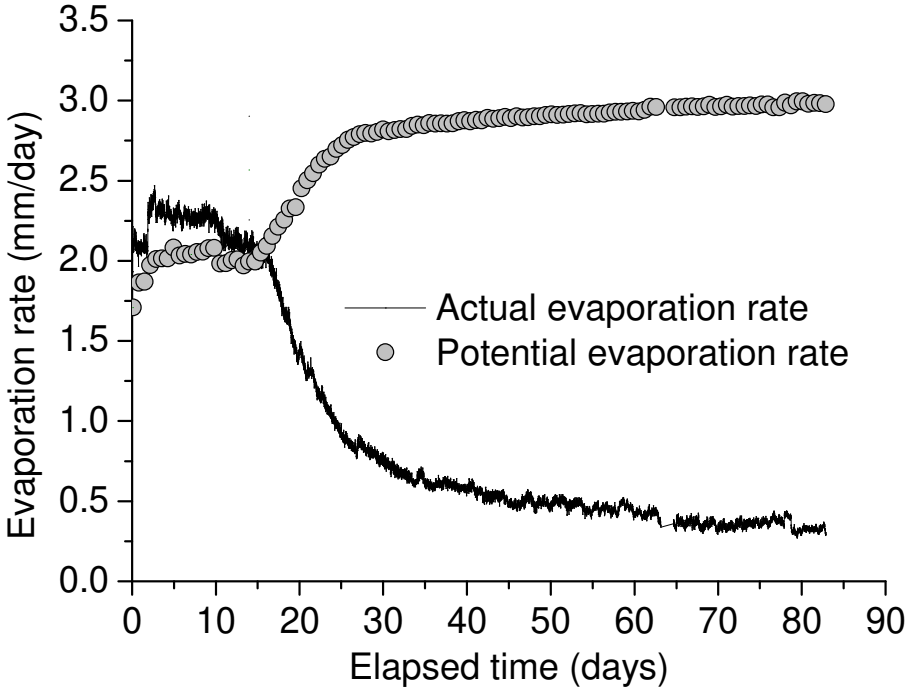

(a)

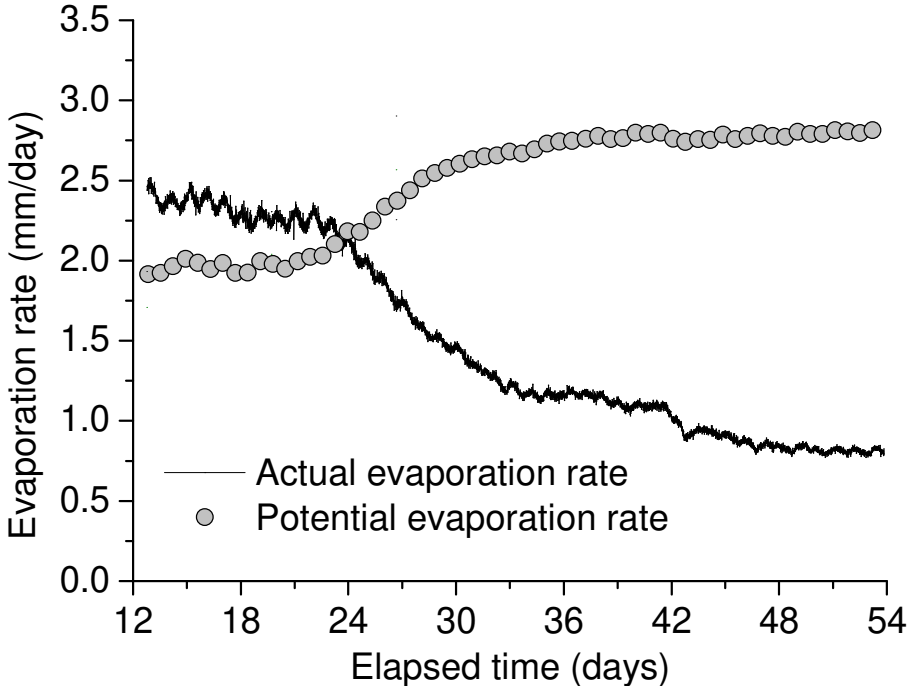

(b)

644 **Fig. 6.** Evolutions of actual and potential evaporation rates: (a) Test 1, (b) Test 2.

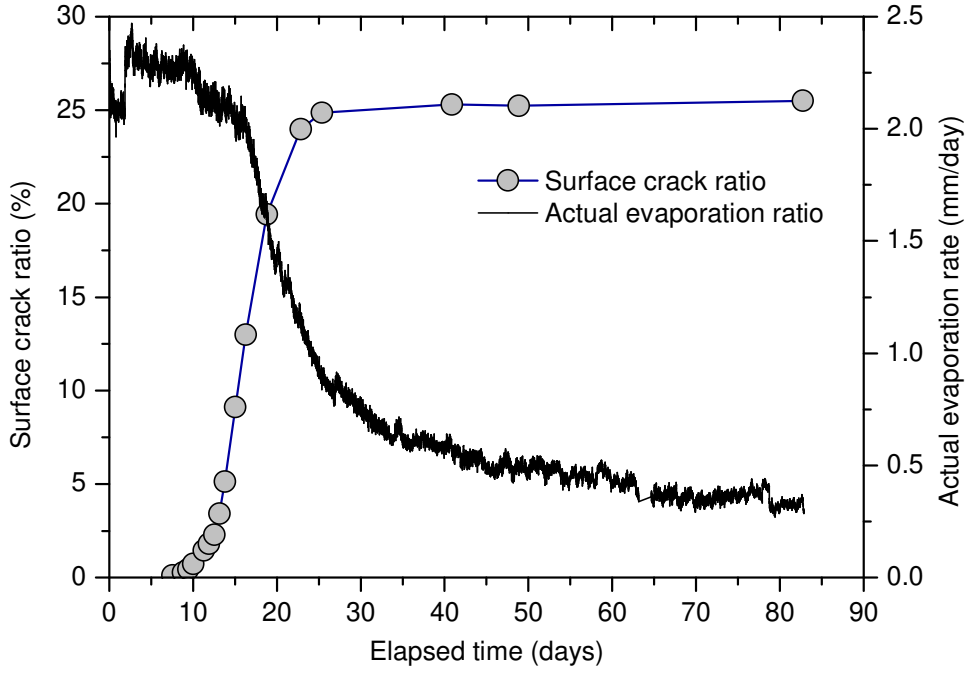

(a)

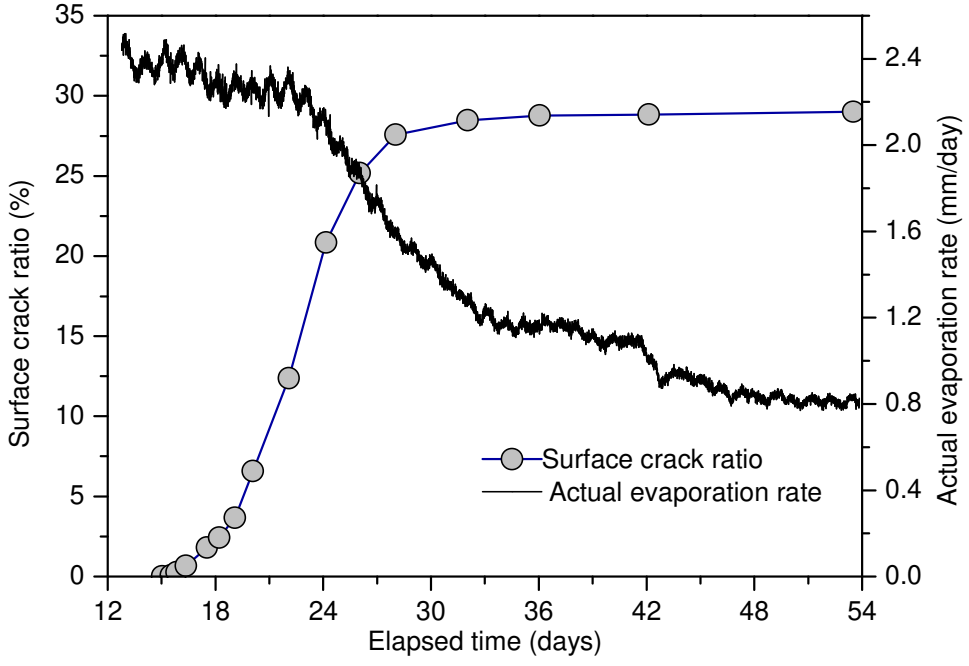

(b)

Fig. 7. Evolutions of actual evaporation rate and surface crack ratio: (a) Test 1, (b) Test 2.

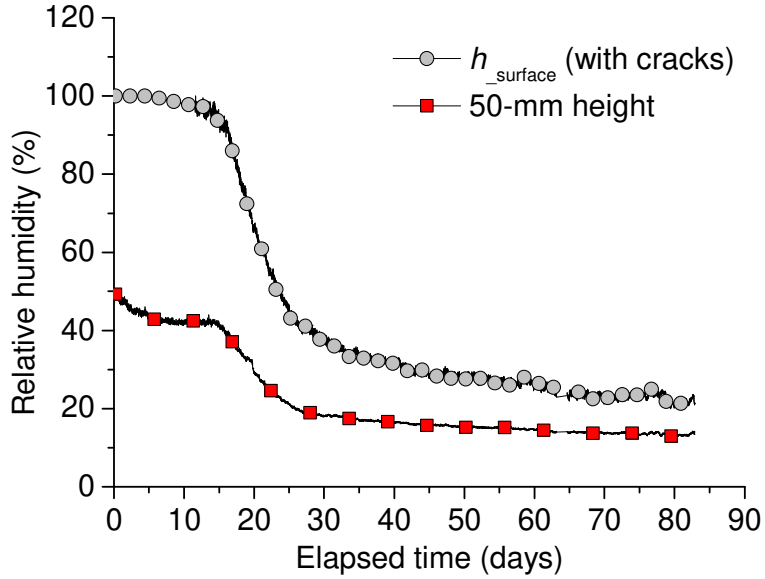

(a)

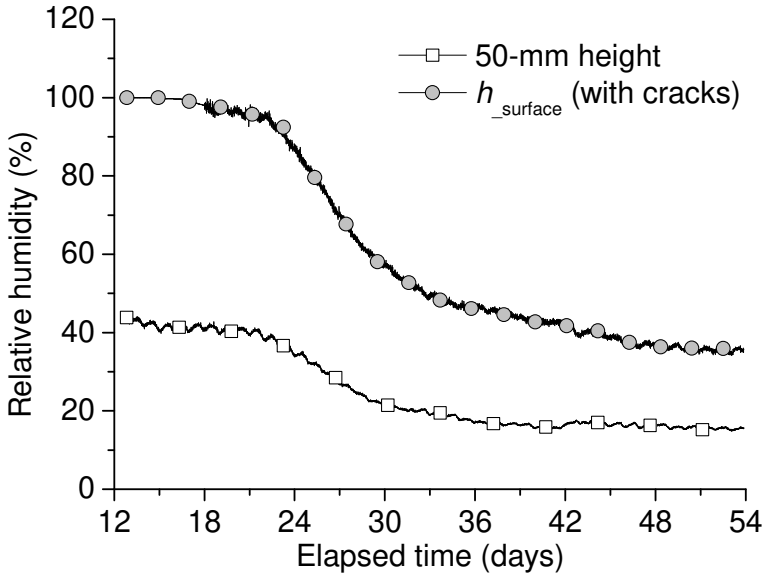

(b)

Fig. 8. Predicted relative humidity at soil surface and the measured one at 50-mm height: (a) Test 1, (b) Test 2.

650

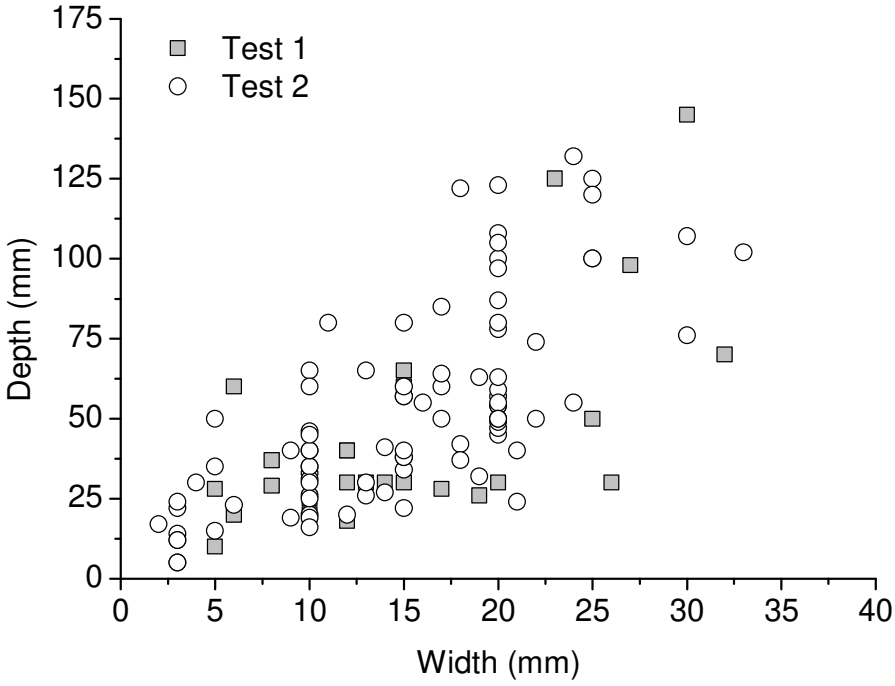

651

652 **Fig. 9.** Depth versus width of crack.

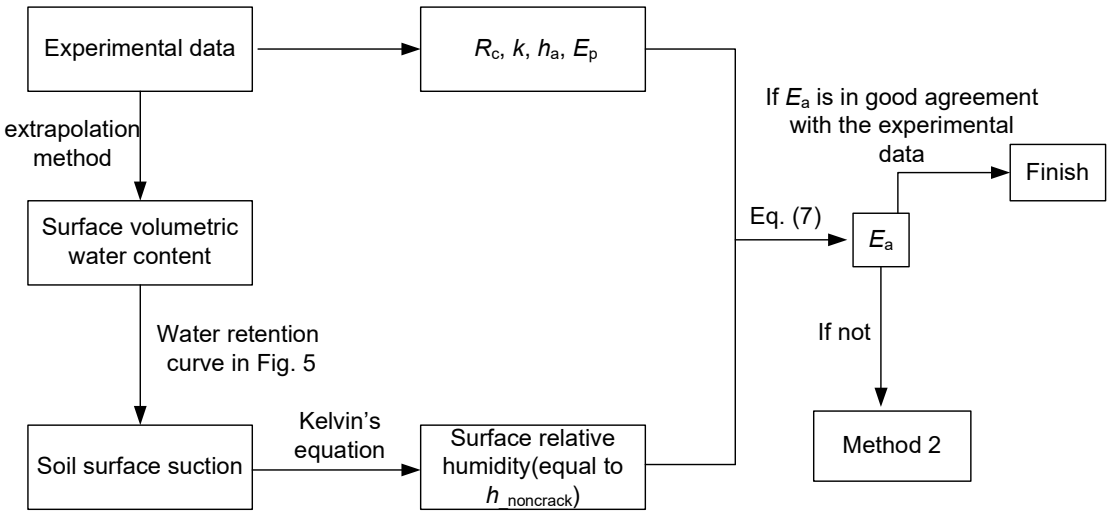

(a) Method 1

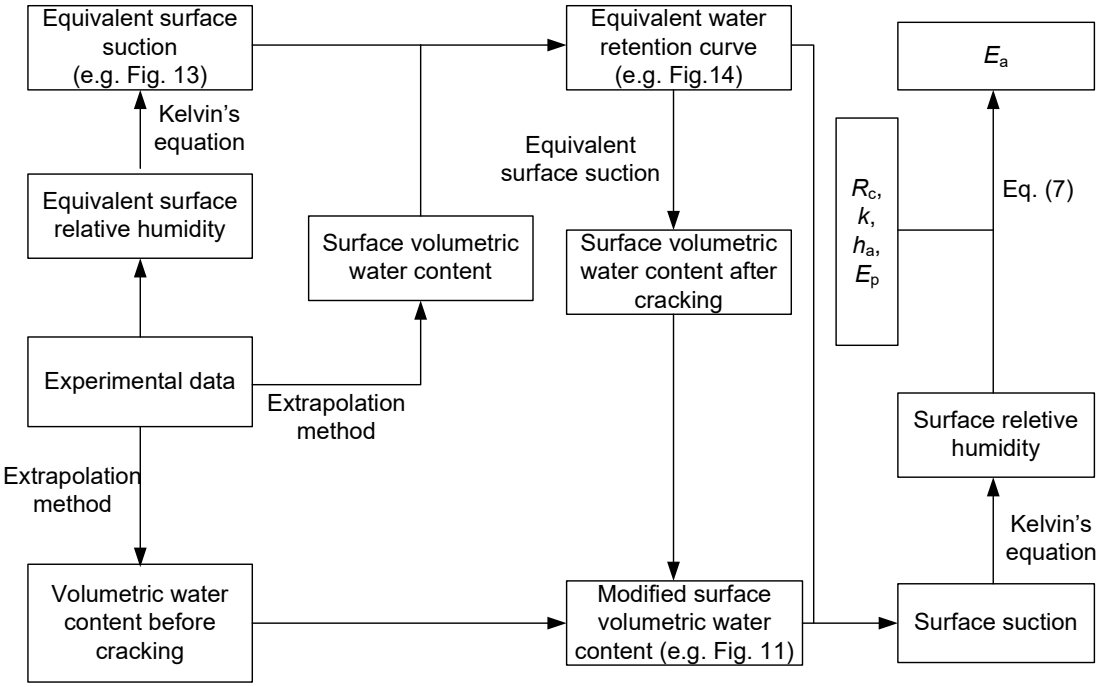

(b) Method 2

Fig. 10. The diagram of the two methods: (a) Method 1 and (b) Method 2.

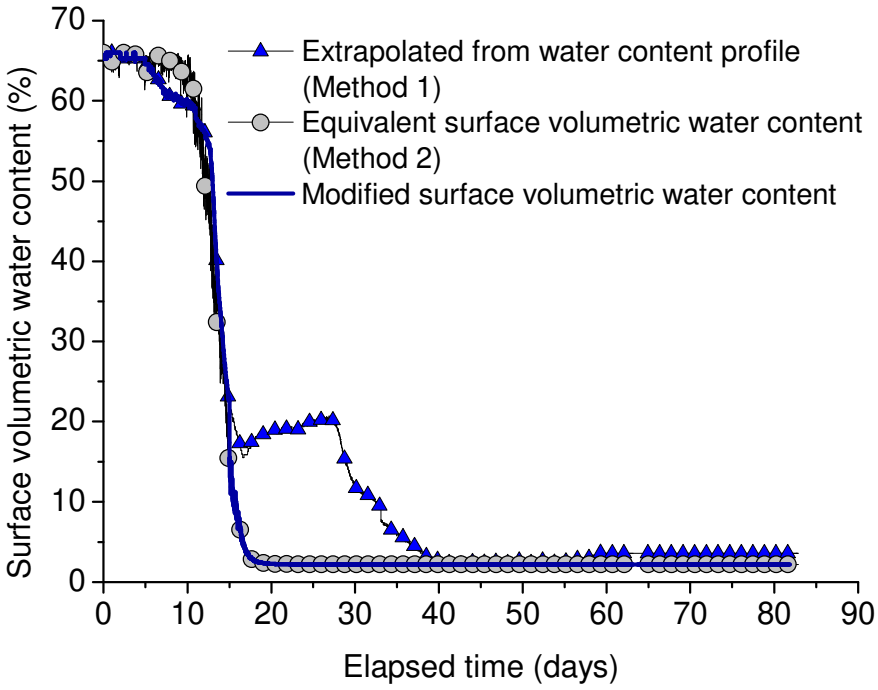

Fig. 11. Surface volumetric water contents determined using Methods 1 and 2 in Test 1.

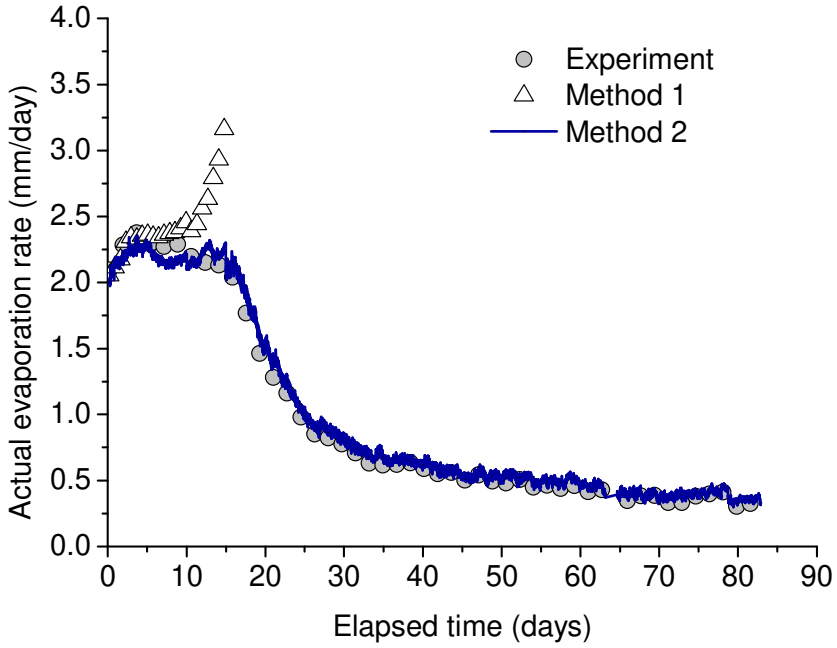

Fig. 12. Prediction of actual evaporation rate by Methods 1 and 2 (Test 1).

665

666

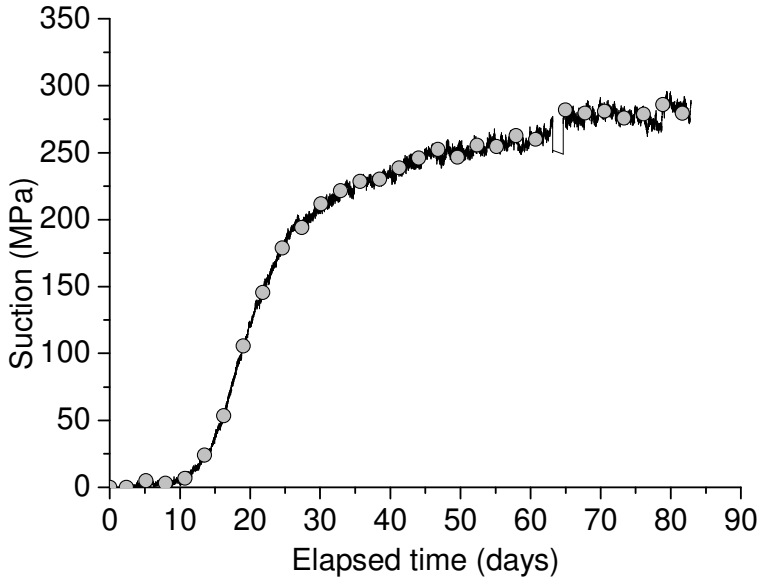

667

668 **Fig. 13.** Equivalent surface suction in Test 1.

669

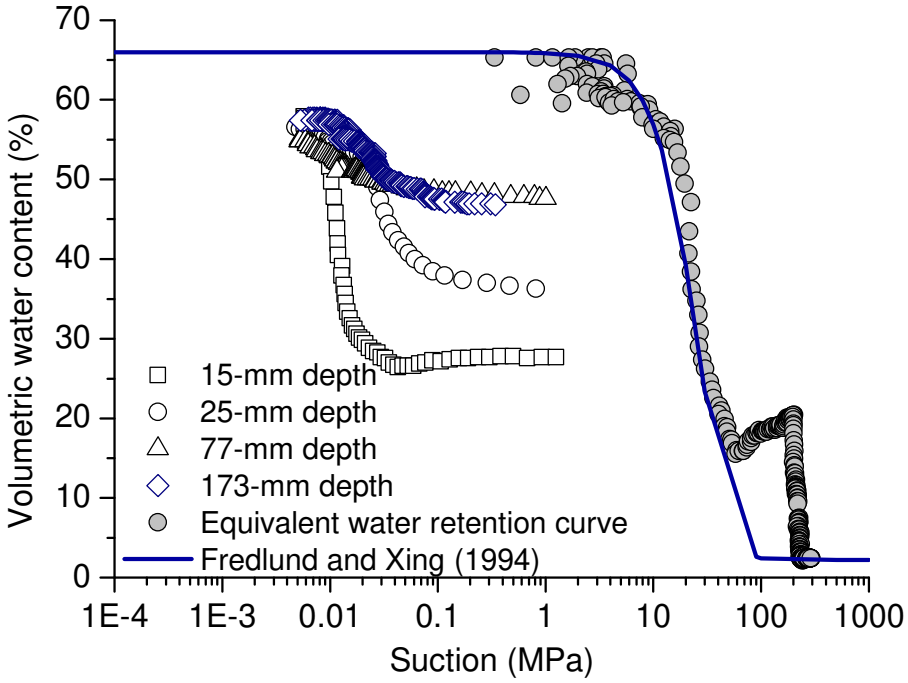

670

671 **Fig. 14.** Equivalent surface water content retention curve in Test 1.

672

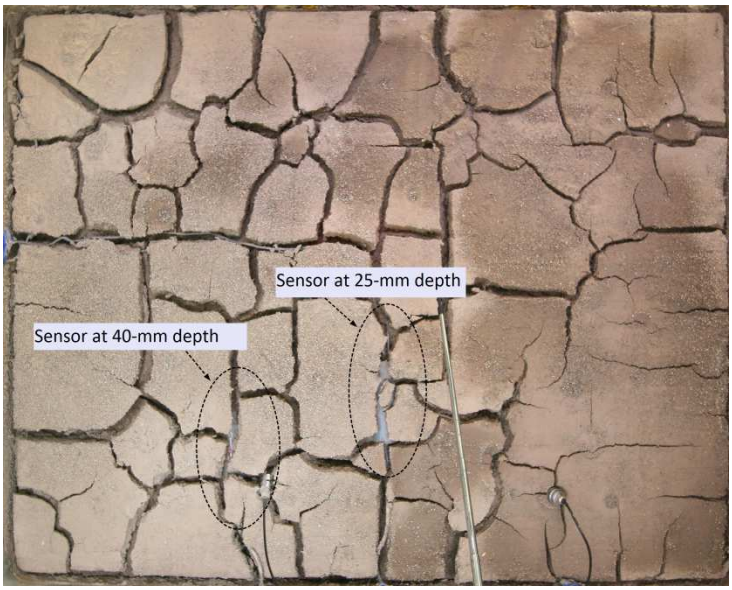

673

674 **Fig. 15.** Typical desiccation cracks during Test 1 (t = 19 days).

675

676

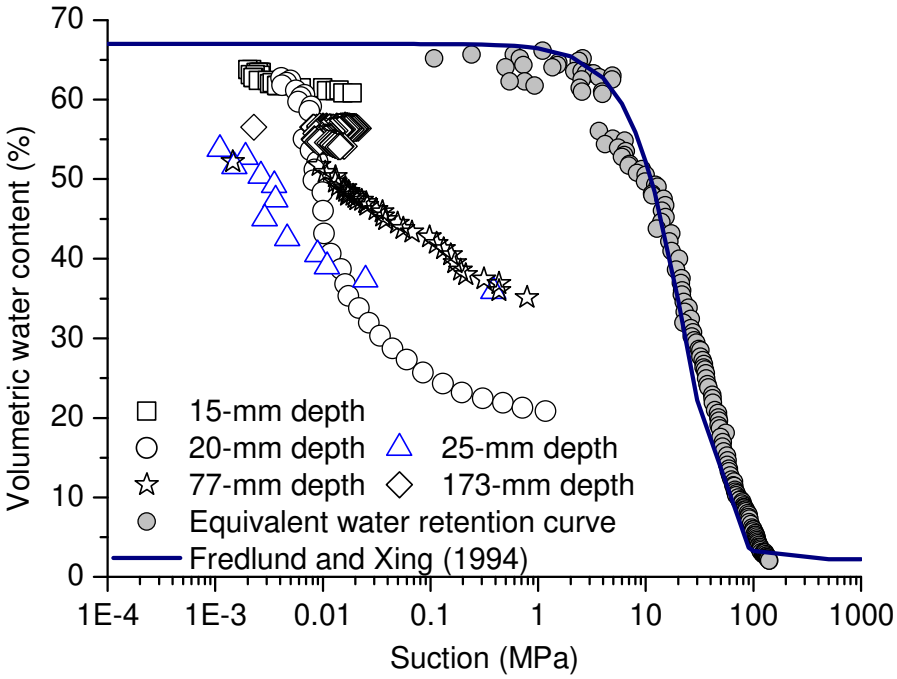

677

678 **Fig. 16.** Equivalent surface water content retention curve in Test 2.

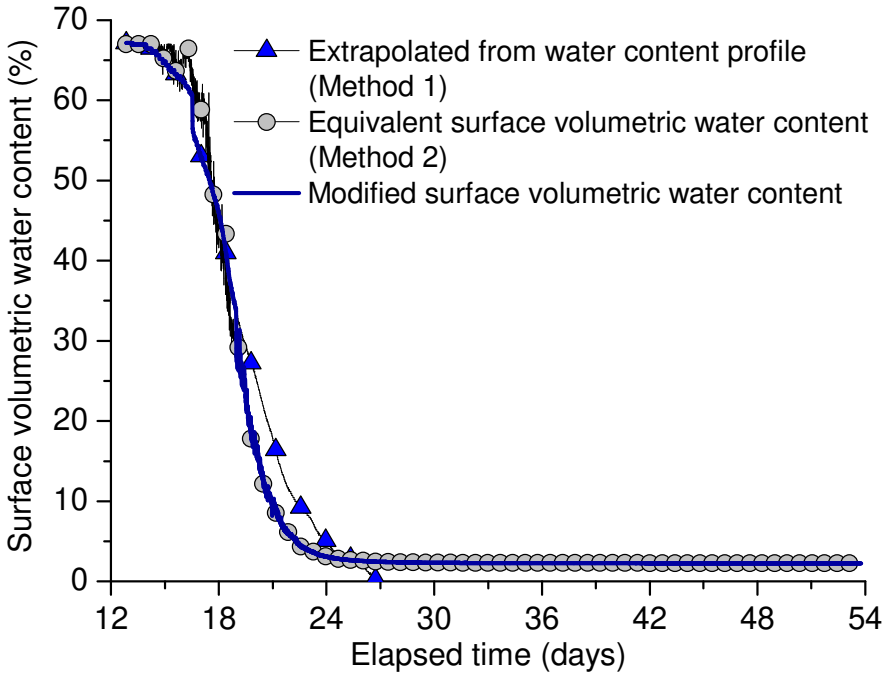

679

680 **Fig. 17.** Surface volumetric water contents determined using Methods 1 and 2 in Test

681 2.

682

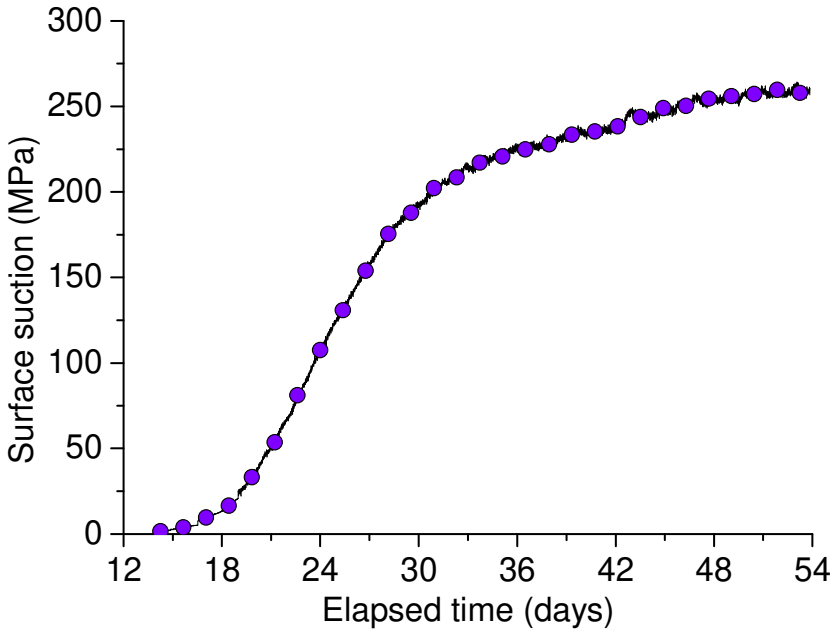

683

684 **Fig. 18.** Surface suction in Test 2.

685

686

687

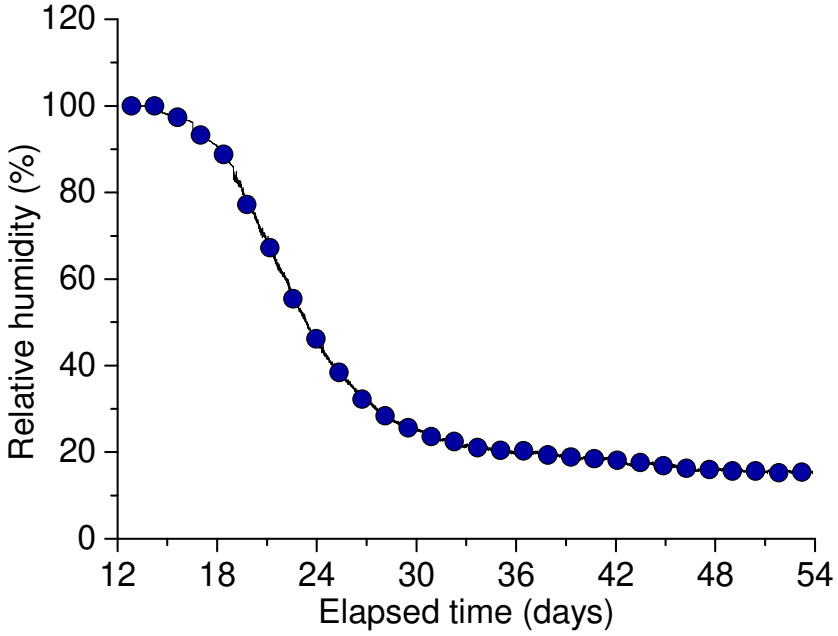

688

689 **Fig. 19.** Surface relative humidity in Test 2.

690

691

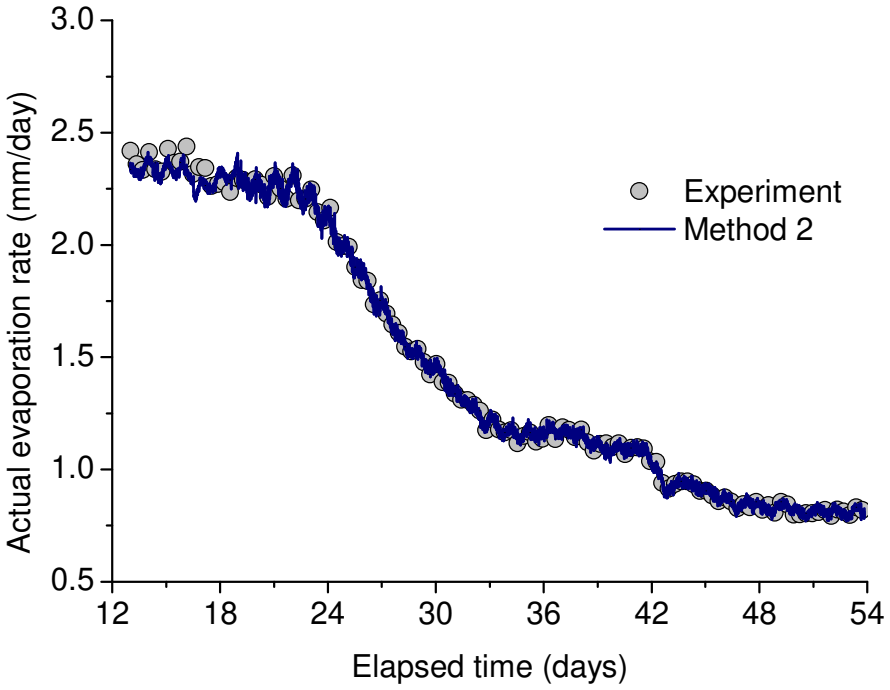

692

693 **Fig. 20.** Comparison between the measured and predicted actual evaporation rates.

694

695